RSC Advances

ROYAL SOCIETY OF CHEMISTRY

www.rsc.org/advances

Nitrogen self-doped carbon nanoparticles derived from spiral seaweeds for oxygen reduction reaction

Fangfang Liu[1,2], Lina Liu[1], Xiuhua Li[1], Jianhuang Zeng[1], Li Du[1,*], Shijun Liao[1,†]

1 Key Lab for Fuel Cell Technology of Guangdong Province & Key Lab of New Energy Technology of Guangdong Universities, School of Chemistry and Chemical Engineering, South China University of Technology, Guangzhou, 510641, China

2 School of Chemical Engineering and Environment, Weifang University of Science and Technology, Shouguang, Shandong, 262700, China

In this work, nitrogen self-doped porous nanoparticles were synthesized through a low cost and simple method with spiral seaweed as a source of nitrogen and carbon. Transmission electron microscopy (TEM), nitrogen adsorption–desorption, X-ray diffraction(XRD), and X-ray photoelectron spectroscopy (XPS) analysis showed that nitrogen was successfully doped into the framework of porous nanostructures. The nitrogen self-doped porous nanomaterial featured a high surface area and micro/mesoporous structures. The fabricated nanomaterial was then used as a metal-free catalyst for oxygen reduction reaction(ORR). This catalyst exhibited improved electrocatalytic activity, long-term operation stability, and high CH_3OH tolerance for ORR in alkaline fuel cells compared with commercial Pt/C catalysts. The influence of different nitrogen species formed in different atmospheres on ORR activity was further investigated. This study shows that spirulina is a suitable nitrogen and carbon source for various carbon-based materials for the development of metal-free efficient catalysts for applications beyond fuel cells.

Key words: biomass-derived metal-free nitrogen self-doped carbon materials oxygen reduction

*Corresponding author, Fax + 86 20 87113586, e-mail: duli@scut.edu.cn
†Corresponding author, Fax + 86 20 87113586, e-mail:chsjliao@scut.edu.cn

reaction

1. Introduction

Fuel cells (FCs) are a promising source of alternative energy because of their cleanliness, high efficiency, usability of exhaust heat, and flexibility for mobile, transportation, and stationary applications. The performance of the cathode in FCs is mainly controlled by oxygen reduction reaction (ORR); as such, efficient ORR electrocatalysts are essential for practical applications of FCs[1-5]. Currently, platinum (Pt) and its alloys are regarded as the optimal catalyst for ORR in FCs. However, the high cost, scarcity, and limited durability of Pt as electrode materials hinder its application for ORR catalysts. As a result, developing doped carbon catalysts for the cathodic reduction of oxygen has emerged as one of the most attractive topics in research on fuel cells[6-19].

Nature provides a nearly limitless source for fabrication of novel artificial materials with special structures, composition, and properties. Nitrogen-doped carbon materials derived from biomass have received considerable attention as ORR catalysts because of their high activity and strong stability[20-31]. Zhao et al.[20] produced N-doped carbon nanodot/nanosheet aggregates with *monkey grass* as the sole material source via a simple hydrothermal process; the fabricated aggregates exhibit improved electrocatalytic activity, stability, and resistance to crossover effects compared with commercial Pt/C electrocatalysts. Wang et al. [21]synthesized a new type of Fe- and N-doped carbon materials through pyrolyzation of ferric chloride doped egg white. The proposed synthesis route is an easy, green, and inexpensive process. The as-prepared sample shows feasible magnetism and comparable ORR activity with commercial Pt/C. Yu et al. [27]reported the pyrolysis of natural seaweed, *Undaria pinnatifida*, as a single precursor, without

any further activation process to obtain a highly porous carbon material as a metal-free efficient electrocatalyst. Our group previously demonstrated a facile and green approach used to synthesize heteroatom-doped biomass-derived carbon materials by using soybean[32] and nori[33] as precursors; the developed catalyst exhibits satisfactory electrocatalytic activity toward ORR.

Spirulina platensis, an abundant and low-cost species, is utilized as food for humans and as a raw material in the pharmaceutical and cosmetic industries because of its high protein content[34]; as such, this organism is a suitable carbon precursor for synthesis of N-doped carbon catalysts for ORR.

In this study, we report a low-cost, simple, and green approach for the synthesis of nitrogen self-doped porous carbon materials from spirulina by using a facial hydrothermal process and pyrolysis in NH_3 atmosphere. Biomass-derived carbon catalysts with a porous structure and a high specific surface area show excellent catalytic ability, stability, and tolerance to methanol poisoning effects.

2. Experimental

Nitrogen self-doped carbon materials were obtained by hydrothermal carbonization of microalga (Spirulina platensis)/glucose(AR).The microalgae/glucose(SP-G) mixture was dispersed in water (15 wt% microalgae and 15 wt% glucose) and stirred for 18 h. The dispersion was then placed into an autoclave with a volume of 50 mL and then treated(H) at 180 °C for 24 h. After the reaction, the autoclave was cooled in a water bath at room temperature. The yellow/brown carbonaceous material was obtained and dried at 80 °C under vacuum overnight. The as-prepared carbonaceous material was annealed under argon

atmosphere and then in NH_3 atmosphere at 900 °C for 0.5 h at a heating rate of 10 °C min^{-1}. The material was then leached in 1M H_2SO_4(A) at 80 °C for 8 h and then annealed at 900 °C for another 0.5 h in NH_3 flow. Sample prepared according to the above procedures was named as SP-G-H-NH_3-A all along the paper. For comparison, the following mixtures were prepared: SP-H-NH_3-A, through the same method without adding glucose; SP-Ar-A and SP-NH_3-A, under argon atmosphere and NH_3 atmosphere without adding glucose and hydrothermal treatment process, respectively.

Electrochemical measurements were conducted in a standard three-electrode glass cell in an electrochemical workstation (Ivium, Netherlands) coupled with a rotating disk electrode (RDE) system (PINE Research Instruments, USA) at room temperature. A glassy carbon electrode (GCE, with a diameter of 5 mm and an electrode area of 0.1964 cm^2) was used as the working electrode substrate, with Ag/AgCl (3M KCl) and Pt wire as the reference and counter electrodes, respectively. A slurry of the active material was prepared by mixing 5.0 mg of the catalyst with 1 mL of an ethanol solution containing Nafion (0.25 wt%) under ultrasonication. Subsequently, 20 mL of the catalyst slurry was pipetted onto the surface of the GCE and then dried under an infrared lamp to form a catalyst film on the GCE substrate. The catalyst loading applied was approximately 0.51 mg cm^{-2}. Linear sweep voltammetry (LSV) measurements were conducted in 0.1 M KOH solution at a scan rate of 10 mV s^{-1}. The chronoamperometric response was obtained at − 0.30 V (vs. Ag/AgCl) in an O_2-saturated 0.1 M KOH solution. During the measurement of the catalyst electrode at -0.30V in an O_2-saturated 0.1 M KOH solution, 2.0 mL mixed solution containing 0.1 M KOH and 3M methanol was injected into ca. 60 mL electrolytes. After that we suspended the instrument for 2 min to fully mix the solution, and then restarted the measurement to record the chronoamperometric response of the catalytic electrode to the addition of methanol[35]. A long-term constant voltage discharge test was also

conducted. The catalyst was discharged at −0.30 V for 30,000 s in O_2-saturated 0.1 M KOH solution by using the chronoamperometric method at a electrode rotating rate of 900rpm.

Transmission electron microscopy (TEM) images were recorded on a JEM-2100 transmission electron microscope (JEOL, Japan). X-ray diffraction (XRD) patterns were obtained using a TD-3500 powder diffractometer (Tongda, China). Specific surface areas and pore size distribution was determined using Brunauer–Emmett–Teller (BET) nitrogen adsorption–desorption on a TristarII3020 (Micromeritics, USA) gas adsorption analyzer. X-ray photoelectron spectroscopy (XPS) was performed on an ESCALAB 250 X-ray photoelectron spectrometer (Thermo-VG Scientific, USA). ICP-AES (Leema PROFILE, America) was used to analyze the contents of trace metal elements.

3. Results and discussion

Fig.1 shows the SEM and TEM images of different carbon materials derived from natural spiral seaweed. The nanomaterial features a slightly rough surface without special morphology when pyrolyzed under argon atmosphere and shows a fluffy porous structure when pyrolyzed in NH_3 atmosphere as shown in Fig.1a and b, respectively. This finding indicates that ammonia gas affects the morphology of the prepared catalyst. Hydrothermal carbonization also affects the morphology of the catalyst samples distinctly. As shown in Fig. 1c, catalyst prepared using pyrolyzed natural spirulina in NH_3 atmosphere after the hydrothermal treatment exhibits uniform nanoparticles with adhesion. The morphology and structure of carbon materials had no obvious changes after adding glucose to the hydrothermal process followed by pyrolysis in NH_3 atmosphere (Fig.1d). The fluffy porous structure of graphite was formed by stacking with

carbon nanoparticles.TEM images (Fig.1e and f) showed that the catalyst owned disordered morphology of porous structure, indicating low graphitization degree. The disorder might be caused by the incorporation of nitrogen, which was consistent with the following XRD results.

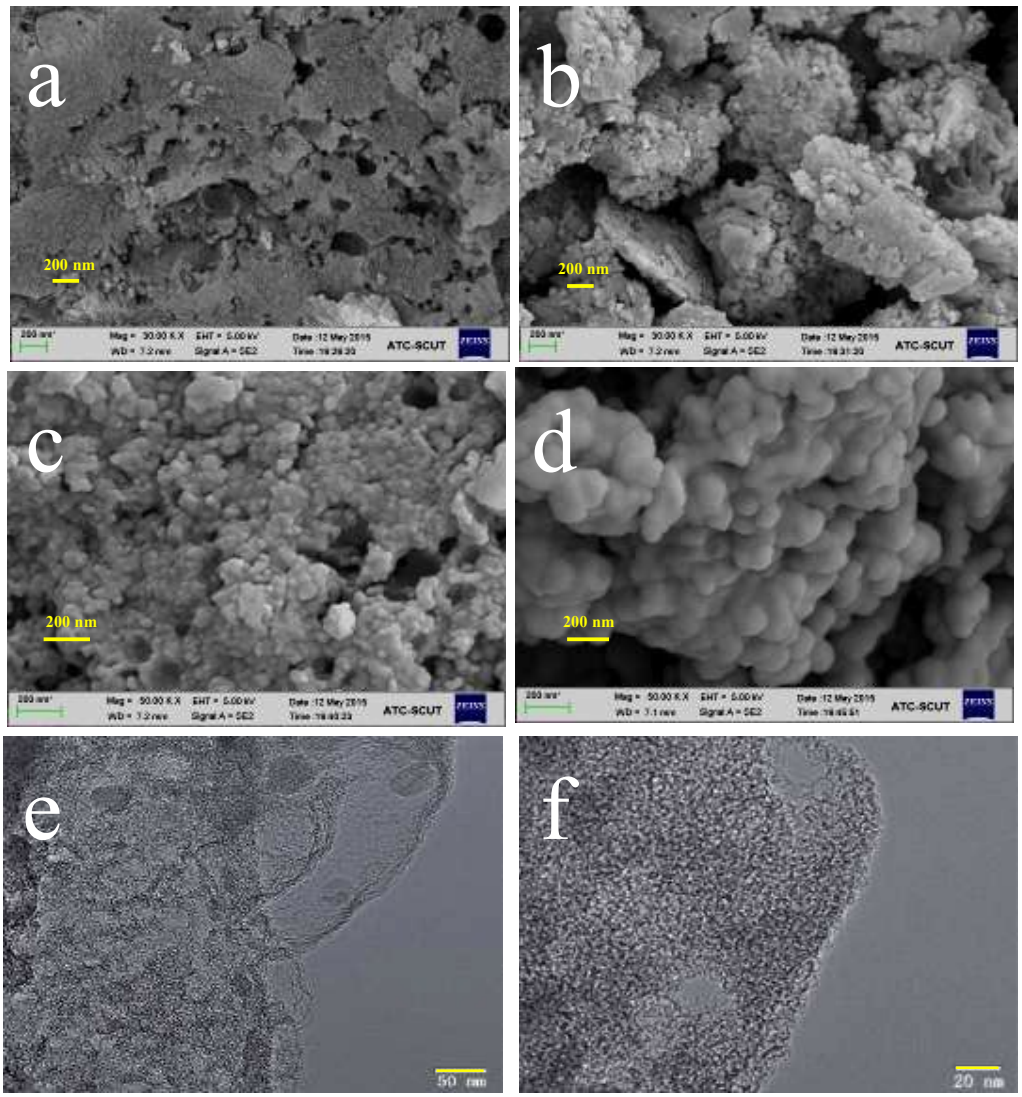

Fig.1 SEM images of (a) SP-Ar-A, (b) SP-NH_3-A, (c) SP-H-NH_3-A, (d)SP-G-H-NH_3-A; and TEM images of (e) and (f)SP-G-H-NH_3-A.

The XRD patterns of all samples are presented in Fig. 2a. At 23.6 °C and 43.5 °C, two typical diffraction peaks were detected; these peaks are assigned to C (002) and C (101),

respectively. With different treating processes, C (002) diffraction peak broadened which indicates that the incorporation of nitrogen would lead to a decreasing of the graphitization degree and therefore to a more amorphous material[36]. All samples show narrow diffraction peaks at 26.6°, as well as at 35.5°, 50.8°, and 60.0°, with increasing peak intensities for NH_3 atmosphere compared with Ar; these peaks may be correlated with C (PDF#26-1080) and CH_4N_{20} (PDF#37-1464), respectively. A certain amount of ammonia was adsorbed on the carbon material surface during pyrolysis in ammonia atmosphere (Fig.1b).

Fig.2b presents the nitrogen adsorption–desorption isotherms and pore size distribution of spirulina-derived porous carbon nanoparticles. From the adsorption isotherm, the characteristic adsorption below a relative pressure of 0.1 is due to the filling of the micropores. SP-G-H-NH_3-A exhibits the highest surface area of 1610.3 $m^2\ g^{-1}$, followed by SP-H-NH_3-A (716.1$m^2\ g^{-1}$), SP-NH_3-A (712.7 $m^2\ g^{-1}$), and SP-Ar-A (199.2 $m^2\ g^{-1}$) (Table 1). The pore size distribution of SP-Ar-A was intensified around 1.2 nm and calculated using the DFT method (Fig. 2b). When the pyrolyzation occurred in NH_3 atmosphere, some mesoporous structures were generated (Fig.2b). After the hydrothermal treatment with glucose, SP-G-H-NH_3-A contained numerous mesoporous structures (2–4 nm), which could be due to the etching effect of ammonia and increased carbon content by glucose addition. Porosity is highly desirable to achieve excellent catalytic performance because it facilitates high mass transfer fluxes and active loading[8]. Therefore, porous carbon nanoparticles are suitable for catalyst preparation. The total pore volume and micropore volume of SP-G-H-NH_3-A are 1.16 $cm^3\ g^{-1}$ and 0.03 $cm^3\ g^{-1}$, respectively. SP-G-H-NH_3-A exhibits the lowest V_{mic}/V_{tot}(0.03) and S_{mic}/S_{BET}(0.15) among all the products (Table 1).Hence, mesoporous structures are advantageous to mass transport

during oxygen reduction.

XPS survey of all samples was performed to determine the electro catalytic activities of heteroatom, and the results are shown in Fig.3. In the N1s high-resolution spectrum of the products, pyridine, prolix, graphitic, and oxidized nitrogen were doped. Peaks at 398.4 , 399.8, 401.3, and 402.2 eve are ascribed to pyridine N species, prolix structure, graphitic N species, and oxidized N species, respectively[37-39]. These results confirm that all products are nitrogen-doped carbon materials. According to the XPS data, the N1s peak shape for the samples significantly changed after paralysis in NH_3 atmosphere. After adding glucose, SP-G-H-NH_3-A showed the highest pyridine N (44.4%) and lowest oxidized N (9.9%) contents compared with the other samples (Fig.2e). The paralysis atmosphere and glucose addition influenced nitrogen atom species, thereby increasing the percentage of pyridine N and reducing the percentage of oxidized N; this phenomenon is predicted to be responsible for the high activity of the nanomaterial [40, 41].

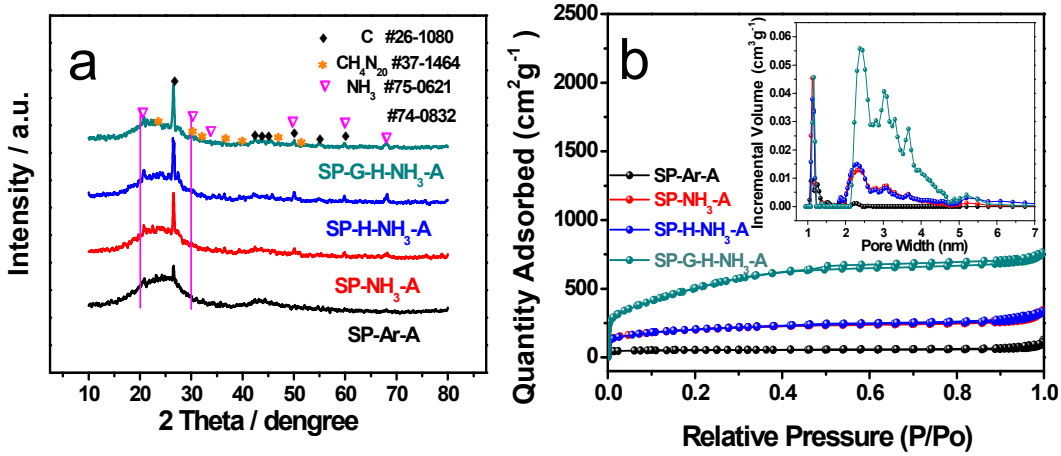

Fig.2 (a)XRD pattern and (b) nitrogen adsorption–desorption isotherms(inset: pore size distribution of all products).

Elementalanalysis results showed that C content in all samples decreased from 72.6 wt%

(SP-Ar-A) to 58.9 wt% (SP-NH_3-A) after pyrolysis in NH_3 atmosphere, which could be due to the erosion of NH_3 into the carbon materials. The C content of SP-H-NH_3-A further decreased to 55.3 wt% because of the decomposition of carbon materials during hydrothermal treatment and NH_3 erosion during pyrolysis. After the addition of glucose, the C content increased to 60.0 wt%. Pyrolysis in NH_3 atmosphere and hydrothermal treatment did not affect the N content, which is about 5.1 wt% in SP-Ar-A, 4.9 wt% in SP-NH_3-A, and 4.5 wt% in SP-H-NH_3-A. This finding could be attributed to the loss of most nitrogen species in the form of liquid or volatile decomposition products. When glucose was added, the N content increased to about 5.3 wt%. We speculate that a certain fraction of nitrogen is fixated via co-condensation reactions involving the microalga- and glucose-derived degradation/hydrolysis products[34].

Table 1: Calculated porosity parameters of all samples.

Samples	S_{BET} (m^2g^{-1})	V_{tot} (cm^3g^{-1})	V_{mic} (cm^3g^{-1})	Micropore area(m^2g^{-1})	V_{mic}/V_{tot}	S_{mic}/S_{BET}
SP-Ar-A	199.2	0.08	0.05	150.3	0.63	0.75
SP-NH_3-A	712.7	0.38	0.08	304.9	0.21	0.43
SP-H-NH_3-A	716.1	0.38	0.07	285.0	0.18	0.40
SP-G-H-NH_3-A	1610.3	1.16	0.03	243.1	0.03	0.15

Fig. 4 shows the Raman spectra of samples. Peaks at ~1310and ~1590 cm^{-1} are assigned to the D and G bands of carbon, respectively. Generally, the D band originates from lattice distortion in sp^2 defects (e.g., vacancy, topological defects, and impurities), and the G band

results from the E_{2g} vibrational mode in the $D4_{6h}$ symmetry group of graphite crystal planes. Therefore, the ratio of the D- and G-band intensities (I_D/I_G) is commonly considered as an indicator of the extent of defects in a doped carbon catalyst[42]. As shown in Fig.3, the peak intensity ratios of the D to G bands (I_D/I_G) are 1.72, 1.88, 1.80,and 1.75 for SP-Ar-A, SP-NH_3-A, SP-H-NH_3-A, and SP-G-H-NH_3-A, respectively. Thus, pyrolysis in NH_3 atmosphere increased the defects of catalyst because of the erosion effect of ammonia.

The ORR catalytic activities of all samples were studied using the RDE test. As shown in Fig.5a, in an alkaline medium, the activity increased with pyrolysis in ammonia atmosphere, and that of SP-G-H-NH_3-A even surpassed that of the Pt/C catalyst, with a half-wave potential of about 35 mV higher than that of the latter. The onset potential for SP-G-H-NH_3-A is about 0.01 V, which is 30mV higher than that of the Pt/C catalyst. The current density at −0.20 V is only 0.20 mA cm^{-2} less than that of Pt/C. As shown in Fig.5b, the SP-G-H-NH_3-A catalyst also exhibited excellent ORR activity in an acidic medium; its limited current density is comparable with that of Pt/C, and its half-wave potential is about 130 mV less than that of Pt/C. Interestingly, neither XPS nor ICP-AES analysis revealed any metal content is found in SP-G-H-NH_3-A. What is the reason for the excellent ORR activity in acidic medium of our catalyst? According to the above analysis, there are probably two reasons for this: first, the high content of pyridinic nitrogen doped within the carbon materials plays an important role in the ORR process; second, a fluffy structure with abundant pores was formed during pyrolysis process in ammonia atmosphere, exposing more active sites in the process of ORR.

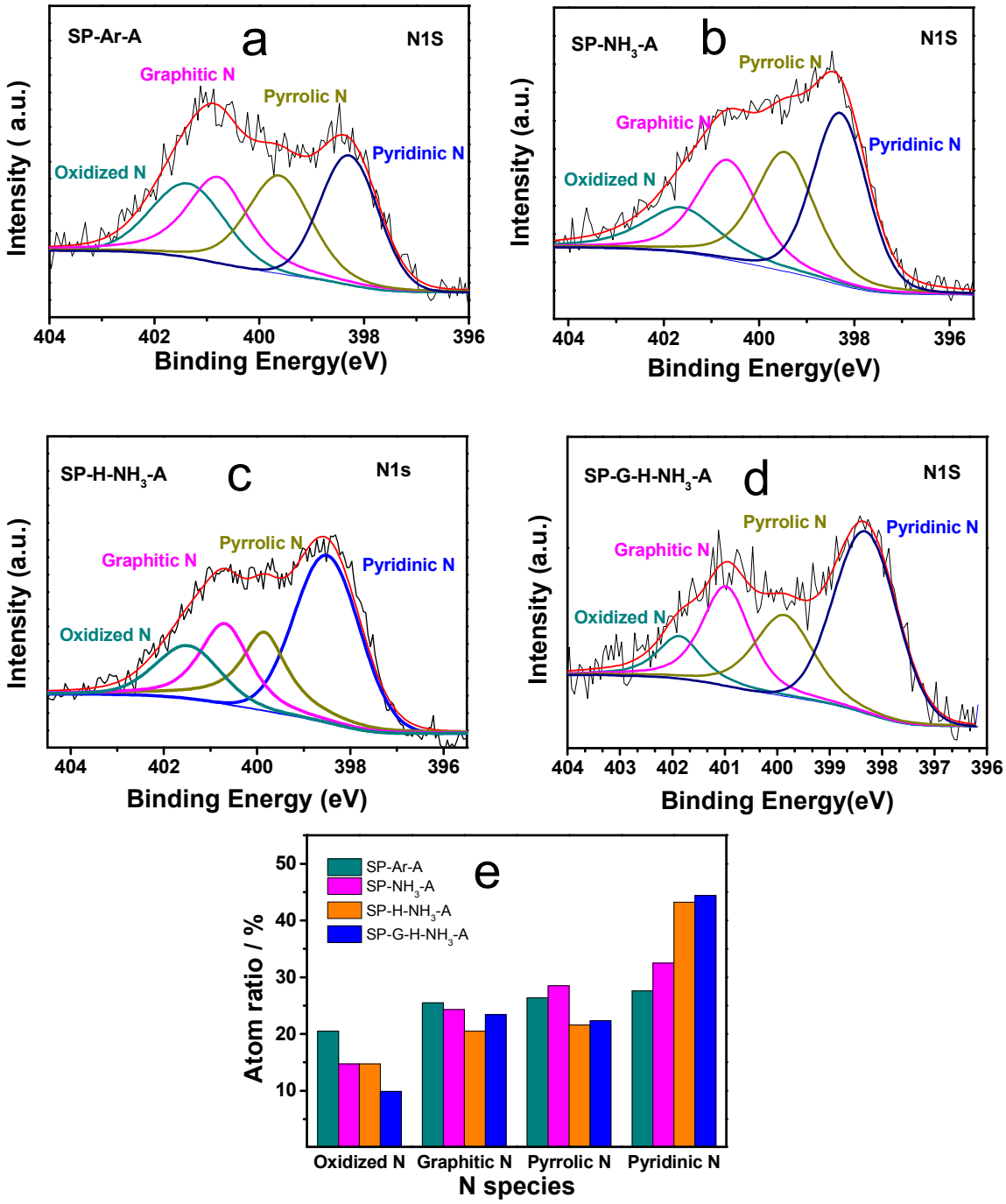

Fig. 3 High-resolution N1s XPS spectra of samples (a)SP-Ar-A, (b)SP-NH_3-A, (c)SP-H-NH_3-A, and (d)SP-G-H-NH_3-A; (e)Content of different types of nitrogen in the as-prepared samples.

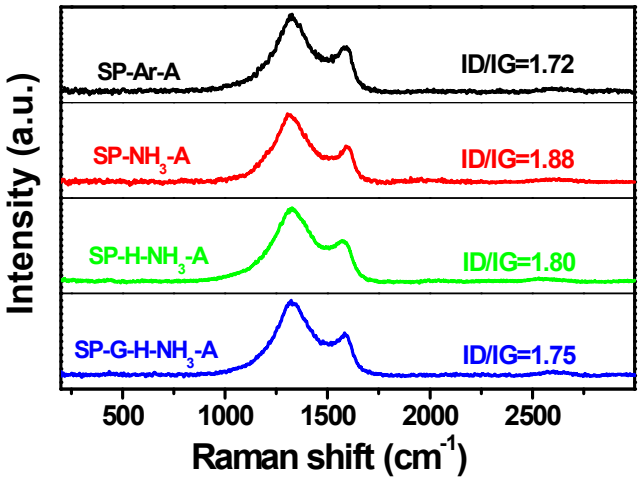

Fig. 4 Raman spectra of different samples.

The reaction kinetics was studied to gain insights into the action of SP-G-H-NH_3-A during ORR. As shown in Fig.5c, the current densities increased with rotation rates because of the shortened diffusion layer. The corresponding Koutecky–Levich (K-L) plots at various potentials displayed good linearity (Fig.5d). Based on calculation from the K-L equation, the electron transfer number per oxygen molecule is close to 4, suggesting that ORR catalyzed by SP-G-H-NH_3-A mainly follows the 4e reaction mechanism.

The catalyst also exhibited excellent methanol tolerance (Fig.5e). When methanol was introduced into the testing cell, the current response of SP-G-H-NH_3-A remained unchanged, indicating its resistance to methanol. By contrast, Pt/C exhibited an instantaneous current jump upon the addition of methanol because of its sensitivity or low tolerance. The excellent tolerance of SP-G-H-NH_3-A makes it a promising cathode catalyst for direct methanol fuel cells (DMFC), in which methanol tolerance in the cathode is essential because of crossover from the anode to the cathode through the membrane.

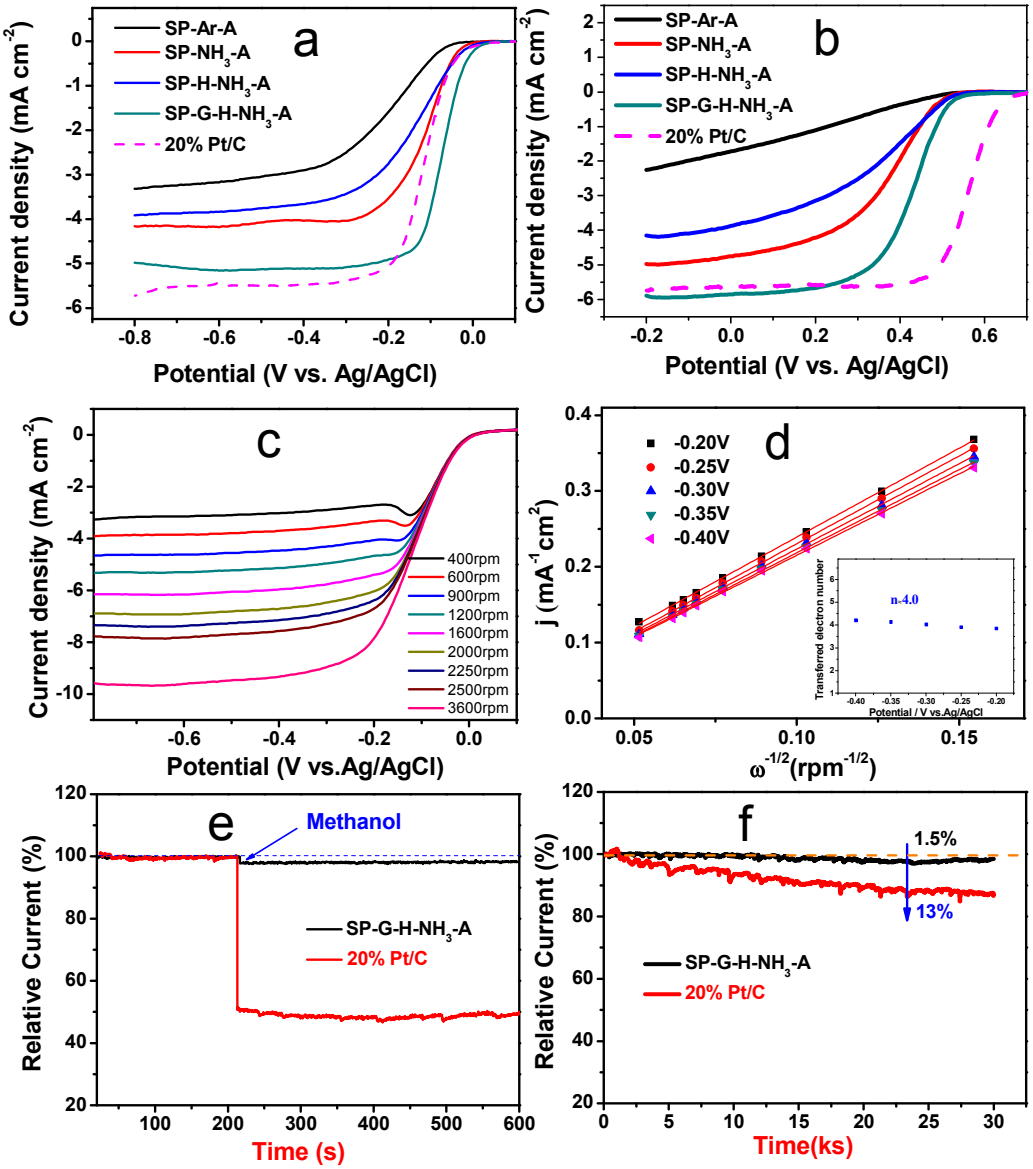

Fig.5 RDE curves of ORR on SP-Ar-A, SP-NH_3-A, and SP-G-H-NH_3-A electrodes in (a) an O_2-saturated 0.1M KOH solution, (b) O_2-saturated 0.1M $HClO_4$ at a scan rate of 10mV/s;(c) RDE voltammograms of SP-G-H-NH_3-A in O_2-saturated 0.1M KOH solution at a scan rate of 10 mV/s with various rotation rates. (d) K–L plots of SP-G-H-NH_3-A electrode[inset of (d) is the dependence of n on potential for the SP-G-H-NH_3-A electrode]. (e) Methanol tolerance tests of SP-G-H-NH_3-A and Pt/C conducted using chronoamperometric response at −0.3V in O_2-saturated 0.1 M KOH aqueous electrolyte (the arrow indicates the introduction of methanol). (f) Long-term durability tests of SP-G-H-NH_3-A and Pt/C by using current–time chronoamperometric measurements at −0.3 V in O_2-saturated 0.1 M KOH solution(relative current(%) means the ratio of the measuring current

density and the initial current density).

Chronoamperometric durability test plots were constructed to evaluate the stability/durability of SP-G-H-NH_3-A (Fig.5f). The current signal decayed about 13% of Pt/C after continuous oxygen reaction (for ca.30,000 s) at −0.3 V, whereas only a slight loss (1.5%) of current density was recorded on SP-G-H-NH_3-A. This finding indicated the high stability of the fabricated catalyst toward the ORR. The nitrogen self-doped porous biomass-derived carbon catalyst may be a promising candidate for the ORR because of its high catalytic activity, stability, and selectivity.

4. Conclusions

A novel nitrogen self-doped carbon material from natural spirulina was synthesized through a facial hydrothermal process and pyrolysis in NH_3 atmosphere. The fabricated catalyst exhibits high ORR activity, as well as good durability and tolerance toward methanol, with activity surpassing that of commercial Pt/C in alkaline medium but slightly less than that of Pt/C in acid medium. Pyrolysis in NH_3 atmosphere can be used to adjust the proportion of nitrogen species. The high activity can be ascribed to the large specific surface area with abundant mesoporous structures, as well as to the high percentage of pyridinic nitrogen and low percentage of oxidized nitrogen. This study demonstrates the feasibility of using natural biomass as a precursor to produce high-performance heteroatom-doped carbon catalysts for applications related to fuel cells and other fields.

Acknowledgements

This work was supported by the National Science Foundation of China (NSFC Project Nos. 21276098, 21476088, 51302091, U1301245), Ministry of Science and Technology of China (Project No. 2012AA053402), and Department of Education of Guangdong Province (Project No. 2013CXZDA003).

References

1. B. C. Steele and A. Heinzel, *Nature*, 2001, **414**, 345-352.
2. C. Wang, H. Daimon, T. Onodera, T. Koda and S. Sun, *Angewandte Chemie International Edition*, 2008, **47**, 3588-3591.
3. M. K. Debe, *Nature*, 2012, **486**, 43-51.
4. R. Cao, R. Thapa, H. Kim, X. Xu, M. G. Kim, Q. Li, N. Park, M. Liu and J. Cho, *Nature communications*, 2013, **4**.
5. Y. Li, M. Gong, Y. Liang, J. Feng, J.-E. Kim, H. Wang, G. Hong, B. Zhang and H. Dai, *Nature communications*, 2013, **4**, 1805.
6. K. Gong, F. Du, Z. Xia, M. Durstock and L. Dai, *Science*, 2009, **323**, 760-764.
7. C. Han, J. Wang, Y. Gong, X. Xu, H. Li and Y. Wang, *J.mater.chem.a*, 2013, **2**, 605-609.
8. R. Wang, T. Zhou, H. Li, H. Wang, H. Feng, J. Goh and S. Ji, *Journal of Power Sources*, 2014, **261**, 238-244.
9. H. Peng, Z. Mo, S. Liao, H. Liang, L. Yang, F. Luo, H. Song, Y. Zhong and B. Zhang, *Sci Rep*, 2013, **3**, 1765.
10. H. Peng, S. Hou, D. Dang, B. Zhang, F. Liu, R. Zheng, F. Luo, H. Song, P. Huang and S. Liao, *Applied Catalysis B: Environmental*, 2014, **158-159**, 60-69.
11. Z. Mo, H. Peng, H. Liang and S. Liao, *Electrochimica Acta*, 2013, **99**, 30-37.
12. Z. Mo, R. Zheng, H. Peng, H. Liang and S. Liao, *Journal of Power Sources*, 2014, **245**, 801-807.
13. C. You, S. Liao, X. Qiao, X. Zeng, F. Liu, R. Zheng, H. Song, J. Zeng and Y. Li, *Journal of Materials Chemistry A*, 2014, **2**, 12240-12246.
14. Z. Liu, H. Nie, Z. Yang, J. Zhang, Z. Jin, Y. Lu, Z. Xiao and S. Huang, *Nanoscale*, 2013, **5**, 3283-3288.
15. Y. Xue, D. Yu, L. Dai, R. Wang, D. Li, A. Roy, F. Lu, H. Chen, Y. Liu and J. Qu, *Phys Chem Chem Phys*, 2013, **15**, 12220-12226.
16. S. Wang, E. Iyyamperumal, A. Roy, Y. Xue, D. Yu and L. Dai, *Angew Chem Int Ed Engl*, 2011, **50**, 11756-11760.
17. J. Xu, G. Dong, C. Jin, M. Huang and L. Guan, *ChemSusChem*, 2013, **6**, 493-499.
18. D. S. Yang, D. Bhattacharjya, S. Inamdar, J. Park and J. S. Yu, *J Am Chem Soc*, 2012, **134**, 16127-16130.
19. S. Jiang, C. Zhu and S. Dong, *Journal of Materials Chemistry A*, 2013, **1**, 3593.
20. H. Zhang, Y. Wang, D. Wang, Y. Li, X. Liu, P. Liu, H. Yang, T. An, Z. Tang and H. Zhao, *Small*, 2014, **10**, 3371-3378.
21. K. Wang, H. Wang, S. Ji, H. Feng, V. Linkov and R. Wang, *RSC Advances*, 2013, **3**, 12039.
22. Z. Yanling, Z. Chengzhou, W. Erkang and D. Shaojun, *Nanoscale*, 2014, **6**, 2964-2970.
23. F. Pan, Z. Cao, Q. Zhao, H. Liang and J. Zhang, *Journal of Power Sources*, 2014, **272**, 8-15.
24. S. Gao, Y. Chen, H. Fan, X. Wei, C. Hu, H. Luo and L. Qu, *Journal of Materials Chemistry A*, 2014, **2**, 3317-3324.

25. P. Chen, L.-K. Wang, G. Wang, M.-R. Gao, J. Ge, W.-J. Yuan, Y.-H. Shen, A.-J. Xie and S.-H. Yu, *Energy & Environmental Science*, 2014, **7**, 4095-4103.
26. J. Lu, X. Bo, H. Wang and L. Guo, *Electrochim. Acta*, 2013, **108**, 10-16.
27. M. Y. Song, H. Y. Park, D. S. Yang, D. Bhattacharjya and J. S. Yu, *ChemSusChem*, 2014, **7**, 1755-1763.
28. C. Zhu, J. Zhai and S. Dong, *Chem. Commun.*, 2012, **48**, 9367-9369.
29. H. Liu, Y. Cao, F. Wang and Y. Huang, *ACS applied materials & interfaces*, 2014, **6**, 819-825.
30. H. Zhu, J. Yin, X. Wang, H. Wang and X. Yang, *Adv. Funct. Mater.*, 2013, **23**, 1305-1312.
31. H. Yang, H. Wang, S. Ji, Y. Ma, V. Linkov and R. Wang, *Journal of Solid State Electrochemistry*, 2014, DOI: 10.1007/s10008-013-2356-0.
32. F. Liu, H. Peng, X. Qiao, Z. Fu, P. Huang and S. Liao, *International Journal of Hydrogen Energy*, 2014, **39**, 10128-10134.
33. F. Liu, H. Peng, C. You, Z. Fu, P. Huang, H. Song and S. Liao, *Electrochimica Acta*, 2014, **138**, 353-359.
34. C. Falco, M. Sevilla, R. J. White, R. Rothe and M.-M. Titirici, *ChemSusChem*, 2012, **5**, 1834-1840.
35. H. Peng, F. Liu, X. Qiao, Z. Xiong, X. Li, T. Shu and S. Liao, *Electrochimica Acta*, 2015, **182**, 963-970.
36. L. Perini, C. Durante, M. Favaro, V. Perazzolo, S. Agnoli, O. Schneider, G. Granozzi and A. Gennaro, *ACS Applied Materials & Interfaces*, 2015, **7**, 1170-1179.
37. D. H. Lee, W. J. Lee, W. J. Lee, S. O. Kim and Y.-H. Kim, *Physical review letters*, 2011, **106**, 175502.
38. M. Zhong, E. K. Kim, J. P. McGann, S.-E. Chun, J. F. Whitacre, M. Jaroniec, K. Matyjaszewski and T. Kowalewski, *Journal of the American Chemical Society*, 2012, **134**, 14846-14857.
39. Z. Chen, D. Higgins and Z. Chen, *Carbon*, 2010, **48**, 3057-3065.
40. S.-Y. Yang, K.-H. Chang, Y.-L. Huang, Y.-F. Lee, H.-W. Tien, S.-M. Li, Y.-H. Lee, C.-H. Liu, C.-C. M. Ma and C.-C. Hu, *Electrochem. Commun.*, 2012, **14**, 39-42.
41. S. Hou, X. Cai, H. Wu, X. Yu, M. Peng, K. Yan and D. Zou, *Energ. environ. Sci.*, 2013, **6**, 3356-3362.
42. Z. Xu and C. Gao, *Nat. Commun.*, 2011, **2**, 571-579.

Graphic abstract

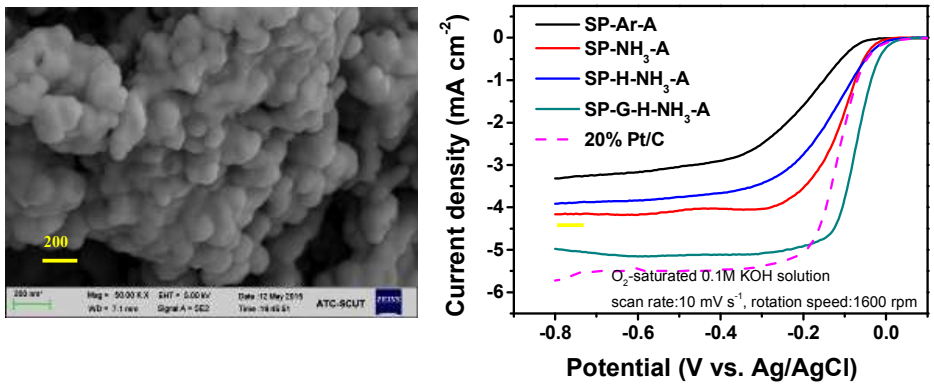

High performance nitrogen self-doped porous carbon materials were synthesized with spiral seaweed biomass as a source of nitrogen and carbon.